Fizika Nizkikh Temperatur, 1996, v. 22, No 2, p. 205–209

Photochemistry of HCl in rare gas matrices

K. Gödderz and N. Schwentner

Institut für Experimentalphysik, FU Berlin, Arnimallee 14, 14195 Berlin, Germany
E-mail:schwent@omega.physik.fu-berlin.de

HCl is dissociated by excitation to the purely repulsive $A^1\Pi$ state and the dissociation fragments are probed via the fluorescence from charge transfer states with the rare gas atom using tunable synchrotron radiation from BESSY (Berlin). The quantum efficiency for the dissociation of HCl monomers in Xe matrices yields a matrix induced barrier of 1.4 eV and a linear increase with excess energy of the H atoms, which agrees with MD simulations. Dissociation of HCl dimers leads to Cl_2 and H_2 formation by two different reaction mechanisms. In the low energy part (1.9 eV < E_{kin} < 4.4 eV), MD simulations suggest a reaction via multidimensional energy surfaces with a quantum efficiency below 1%, which is confirmed by our experiments. In the higher energy part (E_{kin} > 4.4 eV) an impact mechanism is dominant, where the H fragment kicks the H atom off a nearby HCl molecule. Photoinduced and thermal mobilities of H atoms in Xe and Ar matrices were measured. A pathlength for photomobilized H atoms of 19 Å at a kinetic energy of 2.0 eV was estimated from the recombination efficiency of H and Cl atoms by thermal activation. In Ar matrices a H atom pathlength of (21 ± 2) Å at E_{kin} = 2.5 eV was measured from the capture efficiency of codoped Xe traps. From the H loss at 44 K in Xe matrices a thermal diffusion constant of $(7.2 \pm 1.5)\cdot 10^{-13}$ cm^2/s for H in Xe was determined.

1. Introduction

Chemical reactions in condensed matter have wide spread applications and photochemical reactions play a central role [1]. The photoinduced dissociation of a diatomic molecule allows investigation of the most elementary step in these reactions. Excitation of a molecule in the gas phase to a repulsive state leads immediatly to fragmentation. In a solid, dissociation can be hindered by the surrounding atoms, which leads to a reduced dissociation efficiency. This cage effect was first described by Frank and Rabinowitsch [2] and the surrounding atoms constitute the cage. Irreversible dissociation occurs when the fragments leave the original cage, are trapped outside the cage and remain seperated by the cage atoms.

Prototype studies have been started with the photodissociation of hydrides and halogens in van der Waals clusters and solids [3,4]. Rare gas crystals are ideal host materials because they are chemically inert, transparent up to the VUV spectral region, and have a lattice structure of high symmetry (fcc). The periodic lattice structure of the crystal with well defined equilibrium positions is advantageous for Molecular Dynamic (MD) simulations, as compared to the gas and liquid phases. The cage exits are controlled by the mass ratio between the fragment and the host atom, as well as by the molecule-host, fragment-host and host-host pair-wise potentials. MD simulations [5,6] predict two different scenarios for the cage exit of an H atom [3,4]. Trajectories corresponding to a direct cage exit were obtained, where the H fragment escapes after only few collisions and without deforming the cage. In a delayed or indirect cage exit, on the contrary, the H fragment performs many collisions in the cage, displaces cage atoms and exits over the thus reduced energy barrier.

HCl molecules are well suited for the investigation of these types of cage effect, because the first excited state is purely repulsive [7] and dissociation leads to light H and heavy Cl fragments with the excess energy carried away essentially by the H atom. The generated isolated H and Cl fragments can be both probed via fluorescence from excited charge transfer states with the rare gas atoms. HCl molecules tend to form aggregates due to their large dipole moment [8] so that photoinduced dissociation of HCl dimers initiated by excitation to the repulsive state of one of the HCl molecules is studied as a prototype for clusters.

The H atoms are mobilized by the kinetic energy from the HCl dissociation, with the heavy Cl atoms remaining on the original sites of the parent molecules. This photoinduced mobility of H fragments is studied in two ways. In Xe matrices the thermally induced recombination efficiency to HCl was used to derive the original mean separation of the H and Cl fragments induced by the dissociation process. In addition, the diffusion constant D for the thermal mobility was obtained. In Ar matrices the efficiency of formation of XeH centers due to an encounter of the mobile H atom with codoped Xe atoms provides information on the photoinduced pathlength.

© K. Gödderz and N. Schwentner, 1996

2. Experiment

The setup was descriped in detail in Ref. 9 and is only briefly summarized here. The experiments were carried out at the 3 meter Normal Incidence Monochromator (NIM) at the electron storage ring BESSY I in Berlin. The monochromator with a grating of $1200\ mm^{-1}$ and a blaze of 130 nm delivers dispersed radiation in the spectral range from 4 to 20 eV. The light is focused on a LiF substrate, which is cooled with a He flow cryostat. The temperature was varied between 5 and 50 K. A Seya-Namioka and a 0.25 m Ebert Monochromator were used to investigate the flouresence light from the sample in the spectral regions 105–250 nm and 180–1000 nm, respectively. HCl was mixed with the rare gases at partial pressures which were varied from 1 to 0.01% and then condensed onto the cold LiF substrate. HCl with a purity of 99.999% and rare gases with purities 99.9999% (Ar), 99.99% (Kr) and 99.998 (Xe) were used.

Temperature and concentration studies were performed to optimize sample quality and to control HCl aggregation as reported previously [10]. Absorption spectra of HCl doped samples were measured by using a sodium salycilate converter on the back side of the LiF substrate. The dissociation of the HCl molecules in the matrices was initiated by excitation to the purely repulsive $A^1\Pi$ state. This state is little affected by the surrounding lattice atoms [10]. The dissociation efficiency was determined by probing the content of fragments via the charge transfer states of Rg^+H^-, Rg^+Cl^- (Rg = Ar, Kr, Xe) and $Rg^+Cl_2^-$ (Rg = Ar, Kr), respectively [11,12], versus the irradiation dose.

3. Dissociation of HCl monomers in Xe matrices

The positions of the parent HCl molecules in the lattice are known from IR spectroscopy [13] and those of the fragments from absorption and VUV and UV fluorescence spectroscopy [11]. The HCl occupies a substitutional site in the Xe lattice, the Cl atoms remain in the original substitutional site and the H atoms escape to an interstitial site with O_h symmetry. The lowest absorption band of HCl corresponds predominantely to a transition to the repulsive $A^1\Pi$ state [10]. Close to the low energy wing of this band between 5.9 and 6.5 eV a contribution due to the $a^3\Pi$ state can be superimposed. At higher energies a strong additional absorption due to charge transfer between HCl and a matrix atom was observed [10]. The measured dissociation efficiencies are converted into quantum efficiencies of dissociated molecules per absorbed photon by normalizing to the absorption spectra. The full squares in Fig. 1 show the quantum efficiency for H atom production versus the kinetic energy of the H atoms, which follows from the excitation energy upon substracting the HCl binding energy of 4.43 eV. The quantum efficiency rises linearly with kinetic energy within the measurement range about 1 eV wide and an extrapolation to lower energies yields a threshold value of 1.4 eV. The experimental points start with 1.6 eV because the absorption is too low at lower kinetic energies due to the decrease of the Frank-Condon factor in the red wing of the $A^1\Pi$ band. The dissociation efficiencies for H and Cl atoms are similar and no temperature dependence of these efficienies was observed [14] in contrast to the H_2O case [15]. The experimental data are compared in Fig. 1 with results of an MD simulation [16] and the values around 2.5 eV are normalized to each other. The linear increase in the range from 1.5 to 2.5 eV is quite well reproduced in this calculation. The trajectories in this range show an increasing probability for direct cage exit as a function of excess energy and the efficiencies reflect the balance between recombination, direct cage exit and, especially at higher energies, reentry with recombinations. Nonadiabatic transitions from the $A^1\Pi$ state to the ground state potential surface occur with high probability on a subpicosecond time scale, leading to a

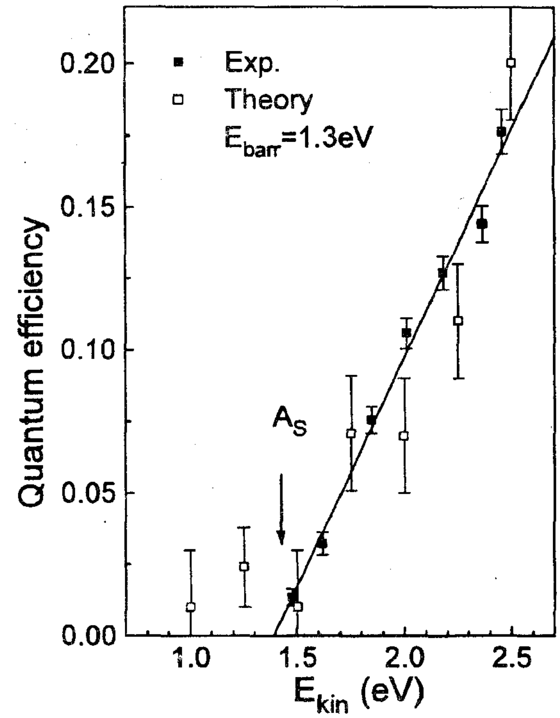

Fig. 1. Experimental (■) and theoretical [16] (□) quantum efficiency at 5 K versus the H atom kinetic energy. A sample with 0.01% HCl in Xe, 100 μm thick and deposited at 40 K was used. Theoretical and experimental values are normalized at 2.5 eV. The solid line is a fit to the experimental data. A_s indicates the onset of absorption.

bination efficiency; dissipation of the excess kinetic energy takes place on this time scale as well. The small but relevant caculated dissociation efficiency for two points below $E_{kin} = 1.4$ eV originates from delayed exit processes which could not be confirmed in experiment owing to the weak absorption. The good agreement above $E_{kin} = 1.4$ eV supports the chosen value of 1.3 eV for the static barrier [16] which differs within the available set of pair potentials.

4. Dissociation of HCl dimers in Ar matrices

An interesting process is the production of Cl_2 molecules due to the dissociation of $(HCl)_n$ clusters or especially $(HCl)_2$ dimers. The Cl_2 photoproduct is probed via the fluorescence of the charge transfer state of $Ar^+Cl_2^-$. The line shape of the Cl_2 vibrational bands of the $A'^3\Pi_{2u}$–$X^1\Sigma^-_{0g}$ transition shows that the Cl_2 molecules occupy a double substitutional site [17] and consequently this has to be the site of the parent HCl dimer.

Three different types of processes can be envisioned: (1) a two-step process of successive dissociation of the two constituents of the dimer by absorption of two photons; (2) a one-step process in which the H atom after dissociation of one HCl has sufficient energy to knock off the second H atom in the cage; and (3) the most interesting concerted one-step process on a potential surface in which the energy gain in the H_2 and Cl_2 formation contributes to the HCl dissociation. The Cl_2 production efficiency in Fig. 2 shows two different regimes within the absorption region of the $A^1\Pi$ transition: one with a kinetic energy threshold around 1.9 eV and with a rather constant efficiency up to 4.4 eV, and another one with a strong increase above 4.4 eV. The high efficiency above 4.4 eV corresponds to the one-step process (2) because the kinetic energy of 4.4 eV of the H atom is sufficient to break up the second HCl molecule in the cage. The binding energy of the $(HCl)_2$ dimer of 431 cm^{-1} [18] can be neglected. MD simulations [19] predict for HCl in Ar clusters also the concerted process (3) and the efficiency observed between 1.9 eV and 4.4 eV in Fig. 2 originates presumably from this process in the Ar matrices. From the energetical point of view the reaction $HCl + HCl \rightarrow H_2 + Cl_2$ is exothermic with an activation energy of 1.5 eV and the energy above the observed threshold of 1.9 eV is sufficient for this process.

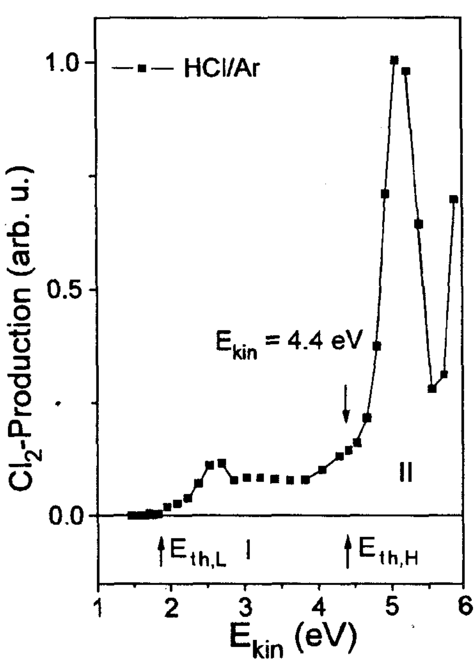

Fig. 2. Production efficiency of Cl_2 in Ar matrix at 5 K in a 0.1% HCl in Ar sample, 500 μm thick, deposited at 23 K. $E_{th,L}$ and $E_{th,H}$ indicate the thresholds for the low and high energy regimes.

5. Thermal and photoinduced mobility of H atoms in Xe and Ar matrices

A microscopic description of a photoreaction in condensed matter has to include the mobility of the fragments besides the cage exit dynamics. This will be the topic of the following part. Photomobile H atoms are again generated in Xe and Ar matrices by dissociation of HCl molecules. The H atoms will be trapped at a certain distance l from the original site after dissipation of their kinetic energy. This distance was derived in two different ways.

5.1. Photoinduced pathlength in Xe matrices

It is well known that the diffusion of H atoms can be thermally activated around 44 K in Xe matrices [20] and this thermal mobility was used to estimate the photoinduced pathlength l of the H atoms. It is expected that l increases with dissociation energy and consequently the probability for geminate recombination with the Cl atom by thermal diffusion should decrease while the H + H recombination efficiency to H_2 should increase, accordingly. The thermally induced loss Δ of Cl and H atoms versus the excess kinetic energy of H atoms by annealing (typical for 10 min) to 44 K is shown in Fig. 3 for two HCl concentrations [21]. The Δ values are normalized to the produced amount of fragments. The H and Cl contents were probed via the fluorescence intensity of the RgH and RgCl charge transfer states.

All H atoms vanish after annealing to 44 K, independent of the kinetic energy and for both concentrations. The Cl atoms show a different behavior . For

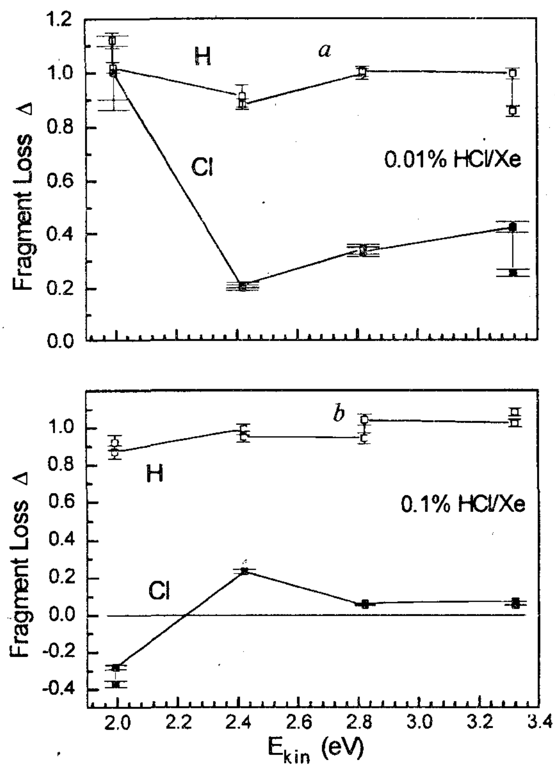

Fig. 3. Normalized losses Δ of H (□) and Cl (■) fragments after annealing to 44 K versus the kinetic energy E_{kin} of the H fragments for 0.01% HCl/Xe (*a*) and 0.1% HCl/Xe (*b*). Samples thickness 100 μm and deposition temperature 5 K.

the 0.1% sample and E_{kin} = 2 eV the number of Cl atoms increases somewhat but all Cl atoms are lost in the 0.01% HCl/Xe sample. For larger E_{kin} the Cl atom loss is about 7% in the 0.1% HCl/Xe sample and 35% in the 0.01% HCl/Xe sample. The differences can be attributed to three competing reactions:

(1) $H + Cl \rightarrow HCl$ recombination

(2) $H + H \rightarrow H_2$ H_2 formation

(3) $H + HCl \rightarrow H_2 + Cl$ Cl production

For 0.01% HCl and E_{kin} = 2 eV, the geminate recombination process (1) of the fragments dominates because H and Cl disappear simultanously. For 0.1% HCl/Xe and E_{kin} = 2 eV, process (2) is dominant because H is lost and the Cl content even increases due to some additional contribution from process (3). Obviously, the probability for geminate recombination at E_{kin} = 2 eV is close to unity for 0.01% and l must be smaller than the mean HCl–HCl separation at this concentration. The reduced mean HCl–HCl separation at the concentration of 0.1% leads to a complete loss of H by H–H recombination and l must be in between the two mean HCl separations yielding for l an estimate of 19 Å [21]. Process (2) dominates at higher E_{kin} for both concentrations because H atoms are lost and Cl atoms survive with high probability (Fig. 3). The balance of processes (1) and (2) depends on concentration. Process (1) is more efficient for larger H–HCl and H–H separations, i.e., the smaller concentration the larger is the loss of Cl (compare data for the 0.01% and 0.1% samples in Fig. 3); the probability for geminate recombination is four times larger in the 0.01% samples than in the 0.1% samples. However, H_2 formation is the most efficient process for both concentrations, so the photoinduced pathlenght l must exceed the mean distance between HCl molecules to allow for the larger probability for H–H encounter in the case E_{kin} > 2 eV.

5.2. *Diffusion constant of thermal activated H atoms in Xe*

The time dependence of the loss of H atoms at 44 K due to thermally activated diffusion follows a $t^{-3/4}$ decay law for E_{kin} = 2 eV in the dissociation process and a t^{-1} decay law for E_{kin} > 2 eV. Simulation of the recombination processes with a random walk model predicts a $t^{-3/4}$ behavior for geminate recombination and a t^{-1} behavior for H_2 formation [22,23]. The crossover in the decay law at E_{kin} = 2 eV agrees with the observations (cf. Sec. 5.1) that geminate recombination occurs for E_{kin} = 2 eV and that for E_{kin} > 2 eV the path length l exceeds the HCl–HCl

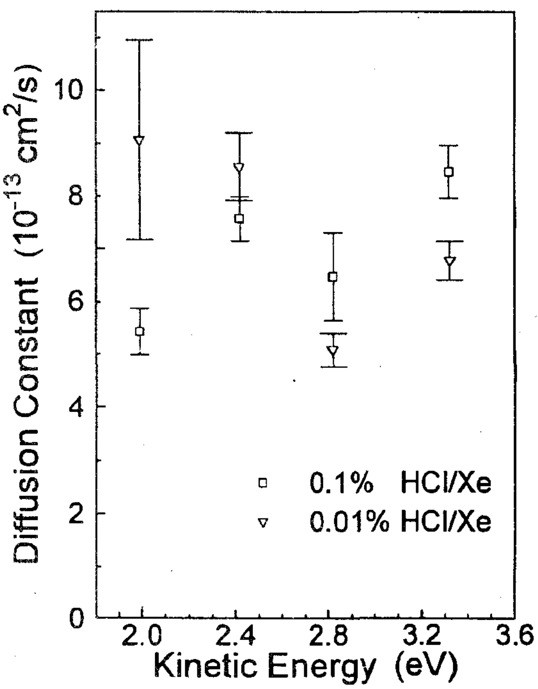

Fig. 4. Calculated H-in-Xe diffusion constant D at 44 K for different kinetic energies of the H atoms for 0.01% HCl/Xe (□) and 0.1% HCl/Xe (▽). The samples as in Fig. 3.

separation, leading mainly to H_2 formation. From this model the thermal diffusion constant D of H atoms in the Xe matrix at 44 K can be calculated (Fig. 4). The diffusion constant D should not depend on E_{kin} since it describes thermally induced motion and the derived mean value of $(7.2 \pm 1.5) \cdot 10^{-13}$ cm^2/s (Fig. 4) is in reasonable agreement with the diffusion constant of $2.6 \cdot 10^{-13}$ cm^2/s obtained from the dissociation data in HBr/Xe system [24] for 40 K. The scatter in Fig. 4 could partly originate from different boundary conditions for different dissociation energies, which was not accounted for in our model.

5.3. Photoinduced pathlength of H atoms in Ar matrices

The photoinduced mobility of H fragments in Ar matrices was determined by introducing Xe atoms as additional traps for H into the 0.01 % HCl/Ar system. The probability of XeH formation should depend on the photoinduced pathlength and on the spacing between the H atoms and the Xe traps and, hence, on the Xe concentration. The probability of XeH formation versus Xe concentration is shown in Fig. 5 for a kinetic energy of 2.5 eV.

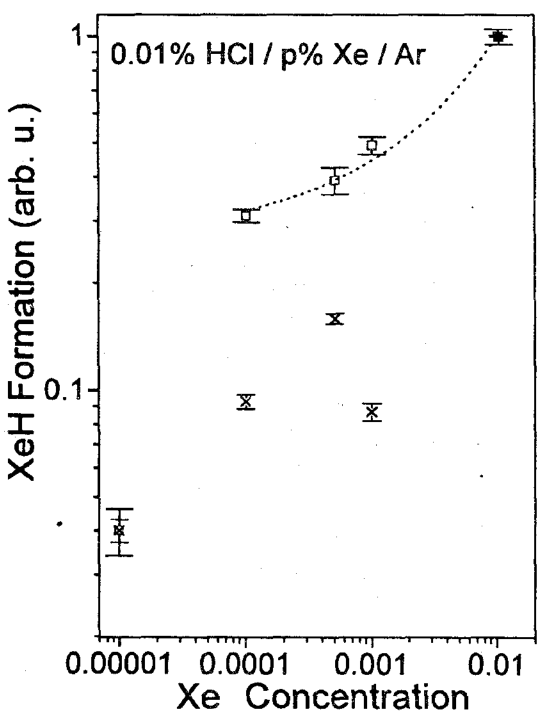

Fig. 5. Normalized XeH (□) and XeCl (X) formation probabilities versus Xe concentration in 0.01% HCl/Ar samples codoped with Xe. Samples of 500 μm thickness deposited at 5 K were used. The samples were irradiated with zero order and a quartz filter in front of the sample corresponding to a mean irradiation energy of 7.1 eV. The dashed curve is a fit to $(b\, t^a + c)$ according to the random walk model with $a = 0.4$ [25]

The experimental data can be explained by a discrete random walk model [25], where static traps are distributed binominally in the lattice. A photoinduced pathlength of (21 ± 2) Å is derived from a fit of the data to this model (Fig. 5). For the 0.00001 Xe concentration the preconditions for applicability of this model are not fullfilled and a lower XeH formation probability is expected in line with the observation. The XeCl formation in Fig. 5 orginates from Xe and HCl aggregates. This contribution can be neglected since it decreases faster at low concentrations.

1. P. Bado, P. H. Berens, J. P. Bergsma, M. H. Coladonato, C. G. Dupuy, P. M. Edelstein, J. D. Kahn, and K. R. Wilson, in: *Photochemistry and Photobiology*, A. Zerwail (ed.), Kluwer Academic Publishers, New York (1982), p. 738; A. L. Harries, J. R. Brown, and C. B. Harries, *Annu. Rev. Phys. Chem.* 39, 341 (1988); J. T. Hynes, *Annu. Rev. Phys. Chem.* 36, 573 (1985).
2. J. Frank and E. Rabinowitch, *Trans. Farad. Soc.* 30, 20 (1934).
3. J. Zoval and V. A. Apkarian, *J. Phys. Chem.* 98, 7948 (1994).
4. N. Schwentner and M. Chergui, in: *Optical Properties of Excited States in Solids*, B. DiBartolo (ed.), Plenum Press, New York (1992), p. 499.
5. R. Alimi, R. B. Gerber, and V. A. Apkarian, *J. Chem. Phys.* 89, 1974 (1988); R. Alimi and R.B. Gerber, *Chem. Phys. Lett.* 173, 393 (1990).
6. I. H. Gersonde and H. Gabriel, *J. Chem. Phys.* 98, 2098 (1993); I. H. Gersonde, Ph. D. Thesis, FU Berlin (1992).
7. M. Bettendorf, S. D. Peyerimhoff, and R. J. Bunker, *Chem. Phys.* 66, 261 (1982).
8. D. M. Lindsay, *J. Phys. Chem.* 86, 3789 (1982).
9. J. Bahrdt and N. Schwentner, *J. Chem. Phys.* 88, 2869 (1988); H. Kunz, J. G. McCaffrey, R. Schriever, and N. Schwentner, *J. Chem. Phys.* 94, 1039 (1991).
10. K. Gödderz, N. Schwentner, and M. Chergui, *preprint*.
11. H. Kunz, J. McCaffrey, M. Chergui, R. Schriever, Ö.Ünal, V. Stepanenko, and N. Schwentner, *J. Chem. Phys.* 95, 1466 (1991)
12. J. G. McCaffrey, H. Kunz, and N. Schwentner, *J. Chem. Phys.* 96, 155 (1992).
13. L. Young and C. B. Moore, *J. Chem. Phys.* 73, 894 (1994).
14. K. Gödderz and N. Schwentner, *in preparation*.
15. E. T. Tarasova, A. M. Ratner, V. M. Stepanenko, I. Ya. Fugol, M. Chergui, R. Schriever, and N. Schwentner, *J. Chem. Phys.* 98, 7786 (1993).
16. I. H. Gersonde and H. Gabriel, *J. Chem. Phys.* 98, 2098 (1993).
17. N. Schwentner, M. Chergui, H. Kunz, and J. McCaffrey, in: *Reaction Dynamics in Clusters and Condensed Phases*, J. Jortner et al. (eds.), Kluwer Academic Publisher (1994), p. 521.
18. J. Serafin, H. Ni, and J. J. Valentini, *J. Chem. Phys.* 100, 2385 (1993).
19. A. B. McCoy, Y. Hurwitz, and R. B. Gerber, *J. Chem. Phys.* 97, 12516 (1993).
20. M. Creuzburg, F. Koch and F. Wittl, *Chem. Phys. Lett.* 156, 387 (1989).
21. K. Gödderz and N. Schwentner, *in preparation*.
22. A. Blumen, J. Klafter, and G. Zumofen, *Models for Reaction Dynamics in Glasses*, in: Optical Spectroscopy of Glasses, I. Zschokke (ed.), Reidel, Dordrecht (1986), p. 199.
23. G. Zumofen, A. Blumen and J. Klafter, *J. Chem. Phys.* 82, 3198 (1985).
24. De LaBrake and E. Weitz, *Chem. Phys. Lett.* 211, 430 (1993).
25. P. Grassberger and I. Procassia, *J. Chem. Phys.* 77, 628 (1982).